

Stress-controlled elastic granular shear flows

By CHARLES S. CAMPBELL

Department of Aerospace and Mechanical Engineering, University of Southern California,
Los Angeles, CA 90089-1453, USA

(Received 16 September 2002 and in revised form 11 April 2005)

While many rheological studies are performed at a fixed concentration, most granular flows are constrained, not by concentration, but by an applied stress. The stress constraint sets the average concentration, but the material is free to vary that concentration slightly to match the applied stress with that generated internally. This study examines stress-controlled systems in light of recent findings that the elastic properties of the particles appear as constitutive parameters even in flowing situations. Stress-controlled flows are shown to behave very differently from flows at fixed concentration. In particular, if the stress is fixed and the shear rate is slowly increased, the flow exhibits the expected progression from elastic–quasi-static to elastic–inertial to inertial flow – a sequence opposite to that followed in fixed-concentration flows. Thus system-scale constraints can have a profound effect on granular rheology.

1. Introduction

Campbell (2002) examined computer simulations of granular shear flows at fixed concentration and found that by including the elastic properties of the particles as a rheological parameter, it was possible to draw out complete flowmaps for granular flows. However, flows at fixed concentration are seldom, if ever, found outside the laboratory. In most common flows such as hoppers and chutes, every point in the material must support an applied stress, usually fixed by a gravitational overburden. The concentration is only approximately fixed by the interaction between this overburden, the flow conditions and material properties. The actual concentration varies slightly to accommodate variations in the local conditions. This paper examines granular shear flows under conditions of controlled stress instead of controlled concentration and fits them into the elastic flow regime structure of Campbell (2002). As will be shown, this change in system-scale constraints has a huge effect on the rheological behaviour of the system as a whole.

2. Background

Classically, granular flows have been studied in two limiting flow regimes. Very slow flows behave quasi-statically in that they generate stresses that are independent of the state of motion. Typically, these are assumed to obey Coulomb's (1773) frictional law and are modelled using plasticity methods (see for example, Jackson 1983). At the other extreme, 'rapid' granular flows behave inertially and generate stresses that vary quadratically with the shear rate (see for example, Campbell 1990). In modelling rapid flows, the particles are likened to molecules in the kinetic theory of gases and are assumed to move thermally and interact by instantaneous collisions. As Coulombic friction opened the formalisms of plasticity theory to model slow flows, these assumptions opened the formalisms of the kinetic theory of gases to model rapid granular flows.

However, little was understood about the parameter space in which these regimes are valid. Furthermore, somewhere between these two extremes, there must be an intermediate regime where inertial effects are important, but the particles are not yet in the thermalized state of rapid flow theory. Campbell (2002) performed computer simulation studies of shear flows at constant volume (i.e. fixed-concentration), and, by including the elastic properties of the particles as rheological parameters, was able to fill out the entire flowmap, connecting the quasi-static and rapid flow regimes.

Campbell (2002) identified two broad regimes and four subregimes for granular flows. In the elastic regimes, particles experience long duration contacts with their neighbours and transmit force through the elastic deformation of the interparticle contacts. This is further subdivided into the elastic–quasi-static (classically called simply the quasi-static regime) where the stresses are independent of the shear rate and the elastic–inertial regime, where the forces associated with flow inertia become comparable with the elastic forces and the stresses vary linearly with the shear rate. In inertial flows, the elastic forces become insignificant, the stresses are generated inertially and vary with the square of the shear rate. Inertial flows are subdivided into the inertial–collisional regime (classically called the rapid-flow regime) in which the particles interact by binary collisions and inertial–non-collisional flows where the particles interact simultaneously with several of their neighbours, but the stresses still scale inertially.

The different behaviours can be more easily understood if we remember that the internal stresses can be thought of as the product: (transported momentum) (transport rate) or alternatively, (average force) (duration of force) (transport rate).

In the elastic regimes, the particles are locked into elastic networks or force chains. Force chains are heavily loaded structures of particles that carry the majority of the load and deform elastically under the applied stresses (Drescher & De Josselin de Jong 1972; Cundall & Strack 1979; Miller, O'Hern & Behringer 1996; Mueth, Jaeger & Nagel 1998; Howell, Behringer & Veje 1999*a, b*). The elastic nature of these stresses is immediately apparent in the photoelastic techniques typically used to visualize force chains experimentally. For the purpose of understanding their effect on the rheology, we can imagine these force chains as nearly linear columns of particles. When compressed, the constituent particles deform at their contact points and the resultant forces are proportional to the stiffness k of the contacts. In a shear flow, stresses are generated when the shear drives particle together to form a chain, compresses, rotates and finally destroys the chain (this process may be clearly seen in videos of the Howell *et al.* 1999*a, b* experiments). In a slow motion at constant volume, the degree of compression and thus the magnitude of the force is determined by the necessity of conforming to a shear motion within the constant volume constraint. Thus the (average force) is independent of the shear rate γ . Chains form as the shear rate forces particles together, with a rate proportional to the shear rate, γ , (which is a time scale for the transport rate), but the chains persist for a time proportional to $1/\gamma$, so that the (force duration) (transport rate) is independent of γ . Thus the product (average force) (duration of force) (transport rate), and therefore all the averaged stresses, are γ independent and the general behaviour is quasi-static. As the degree of compression of the chains is dictated by geometric constraints, the generated forces are related to the elastic properties through the interparticle stiffness, k . This is the elastic–quasi-static subregime.

When the shear rate is large enough, the particle momentum becomes significant and is reflected in the forces generated in the chain. As the inertial part of the particle momentum is proportional to γ , the magnitude of the average force will have the

form $a + b\gamma$ where a is the baseline quasi-static elastic force (i.e. the force as $\gamma \rightarrow 0$) and γ is the extra force arising from the particle inertia. Once again the chains are generated at a rate proportional to γ and persist for a period proportional to $1/\gamma$ so that the (force duration) (transport rate) is again independent of γ . Thus the resultant stresses vary only with the generated forces and increase linearly with γ . This is called the ‘elastic–inertial’ regime as the stresses are generated both elastically and inertially. In their underlying physics, the elastic–quasi-static and elastic–inertial regimes are identical. They are differentiated only because in the elastic–quasi-static regime the inertial forces are negligibly small.

In pure inertial flows, the particles have broken free of the force chains. In that case, the rate at which particles are driven together is proportional to the shear rate γ . However, as the duration of interparticle contacts is determined by how long it takes the elastic contact forces to drive the contacting particles apart, it depends only on the elastic properties of the particles, not on the shear rate. For collisions between only two particles, that duration is the binary collision time, T_{bc} . If more than two particles interact simultaneously, the collision times can be longer than T_{bc} , but will generally be of the same order of magnitude as T_{bc} . (In Campbell 2002, the longest inertial contacts were of the order of $10T_{bc}$. In comparison, when the material was exhibiting elastic behaviour, the duration was proportional to $1/\gamma$ and was independent of T_{bc} ; cases were observed that reached nearly $1000T_{bc}$.) Thus for inertial flows, the rate is proportional to shear rate γ . At the same time, the momentum transferred is proportional to the impact velocity which is also proportional to γ . Consequently, the (transported momentum) (transport rate) is proportional to γ^2 . Thus, the stresses vary quadratically with the shear rate (a behaviour first deduced by Bagnold 1954). One of the most fundamental assumptions of rapid flow theory is that particles interact solely by binary collisions, the inertial regime is further subdivided into an inertial–collisional (or rapid flow regime) and an inertial–non-collisional regime where the particles are in contact with multiple particles simultaneously and rapid flow assumptions do not apply.

There have been attempts to fill in the flowmap. Babic, Shen & Shen (1990) constructed a flowmap for two-dimensional flows of disks, dividing the space between the rapid and what they called their quasi-static regimes, with two transitional regimes (type A and type B) based on the coordination number, the number of simultaneous contacts experienced by a particle. Because different criteria are used for differentiating the regimes, these categories are fundamentally different from Campbell’s four regimes. For example, their quasi-static regime corresponded not to cases where the stress was independent of shear rate, but to cases where force chains were permanent, and only occurred at concentrations near to or exceeding the maximum hexagonal packing of disks; there, the material does not shear uniformly, but slips along surfaces called slip-planes. This does not correspond to any of the cases studied in Campbell (2002) which all occurred at concentrations below random close packing of spheres (which is significantly smaller than the maximum sphere packing). The Babic *et al.* type B transitional regime described cases where force chains formed and broke and thus encompassed both the elastic–quasi-static and elastic–inertial regimes of Campbell (2002). Aharaonov & Sparks (1999) divided the flows into ‘solid’ (inertia-free flows corresponding to the elastic–quasi-static regime) and ‘gases’ (all flows showing inertial effects corresponding to the elastic–inertial, inertial–non-collisional and inertial-collisional flows of Campbell 2002; thus some of their ‘gas’ flows contained force chains). They described their solid/gas transition as a ‘rigidity transition’ although their data indicates and the current results

show, that force chains exist, and thus the material is 'rigid' on both sides of the transition.

As suggested by the choice of names, it has generally been assumed that if we increase the shear rate from zero, we would initially see quasi-static behaviour at low shear rates and eventually reach rapid flow (inertial-collisional) behaviour at high shear rates. But that was not the behaviour observed at fixed concentration by Campbell (2002). In fact, there was no path between elastic–quasi-static and pure inertial flows, simply by varying the shear rate; such a transition was only possible by reducing the concentration. Part of this should be evident. The elastic–quasi-static and elastic–inertial regimes depend on the existence of force chains whereas inertial regimes depend on their absence and we would not expect force chains to vanish when the shear rate is increased. However, inertial flows can be reached by decreasing the concentration below the level at which force chains form. Campbell observed that collisional flows could only be obtained at low shear rates, implying, ironically, that rapid flows are less rapid than other flows. At very large shear rates, the particles may be brought together at a rate comparable to the rate at which they are elastically driven apart, forming force chains at concentrations that would otherwise exhibit inertial behaviour; thus it is possible to have an elastic–inertial \longleftrightarrow inertial transition by changing the shear rate, but not an elastic–quasi-static \longleftrightarrow inertial transition.

However, we might anticipate a different behaviour in controlled-stress flows for which the volume is allowed to change in order to balance an applied stress. At small shear rates, we expect the material to shear at the 'critical state' void fraction appropriate to the stress loading (Casagrande 1938; Roscoe, Schofield & Wroth 1958; Schofield & Wroth 1968). As the shear rate is increased and inertia becomes important, we would expect the system to expand, eventually adopting inertial behaviour when the concentration falls below the value at which force chains form. Hence, if increasing the shear rate in controlled-stress flows, the system should progress from elastic–quasi-static \rightarrow elastic–inertial \rightarrow inertial-non-collisional \rightarrow inertial-collisional behaviour in the expected manner.

Aharonov & Sparks (1999) also considered fixed concentration and fixed-stress separately and noted differences and similarities between them. Their results will be discussed in greater detail later.

The difference between controlled-volume and controlled-stress measurements is reflected in the long observed differences between drained and undrained tests in soil mechanics. In undrained tests, the soil is generally saturated with water which, as the name suggests, is not allowed to drain in or out during the test. The water acts like an incompressible fluid and thus keeps the volume constant throughout the test. Even if the soil structure breaks down, the water pressure can support the applied load and allow the particles much the same freedom of motion as seen in fluid-free constant-volume simulations. However, if the water is allowed to drain away, the fluid will be forced out before it can build up enough pressure to support the applied forces; in those cases the forces must be supported by the particle forces and thus behave in a controlled-stress manner.

We might expect that rheological properties derived at fixed concentrations are still applicable to controlled-stress cases with slight variations in concentration, but as suggested by the above, and as will be shown in the following, this is not the case. Instead it appears that these types of system-scale constraints have a profound effect on the granular rheology.

Portions of this work are presented in Campbell (2004a–c).

3. Computer simulation

These studies were performed using a soft-particle computer simulation, a technique originally developed by Cundall & Strack (1979). (See the reviews of computer simulation techniques by Campbell 1986, 1997 and Herrmann & Luding 1998). As in Campbell (2002), contacts are modelled as a spring with associated stiffness k in the direction along the line connecting the particle centres. A viscous dashpot with coefficient D , is added in parallel to the spring to dissipate the collisional energy. Tangential to the surfaces at the contact point, the particles are connected through a frictional slider with coefficient μ , connected in series with another spring also with stiffness k . This contact model was first used by Cundall & Strack (1979).

The dashpot coefficient D , will be expressed dimensionlessly as a binary coefficient of restitution ϵ (which is the ratio of recoil to impact velocity for a binary collision in the centre of mass frame):

$$\epsilon = \exp \left[-\frac{\pi D}{\sqrt{2mk - D^2}} \right], \quad (3.1)$$

where m is the particle mass. Even though there are few collisional flows of concern to this paper, the coefficient of restitution is still used as it is a convenient dimensionless representation of the particle inelasticity, and has an easily understood physical meaning. Campbell (2002) showed that ϵ appropriately scales the dashpot coefficient D , in the sense that ϵ is the only governing dimensionless parameter containing D and that flows for which ϵ and all other dimensionless parameters are fixed produce quantitatively the same results, regardless of the value of D . (See §4 for a discussion of the governing dimensionless parameters.)

All of these simulations model one thousand spheres of diameter d , confined in a control volume initially dimensioned $10 \times 10 \times 10$ mean particle spacings and bound in all directions by periodic images. (Tests of the effects of control volume size were performed in Campbell, 2002, and showed there was no effect of control volume size as long as the volume is $7 \times 7 \times 7$ spacings or larger, at least for the large particle concentrations of interest here. More limited tests confirm those results for controlled-stress situations.) To induce a uniform shear within the control volume, periodic images above and below the control volume in the y -direction are set in motion with fixed velocity in the manner originally used by Lees & Edwards (1972), which produce a constant shear rate and a constant solids fraction across the control volume. In the following, x is used to represent the direction of the mean motion, y is the coordinate in the direction of the velocity gradient (so the shear-rate $\gamma = |du_x/dy|$, where u_x is the mean velocity in the x -direction), and z represents the out-of-the-shear-plane coordinate (i.e. the vorticity direction).

The stress on the system was controlled by increasing or decreasing the size of the control volume as required to balance the internal stress (which is assessed at each time step) with the applied stress. Conceivably, this could be done in many ways, but for these studies, it was decided to use coaxial shear cells, rectangular chutes and landslides as model systems and allow the control volume to expand only in the vertical direction (the direction of the velocity gradient). The simulation control volume is schematically represented in figure 1. A stress τ_0 is applied in the vertical (y) direction and the control volume expands or contracts as necessary in that direction to balance that stress. Now there are many possible ways in which to move the boundary in response to an imbalance between the applied stress and the stress response generated in the material. As this paper primarily concerns dense

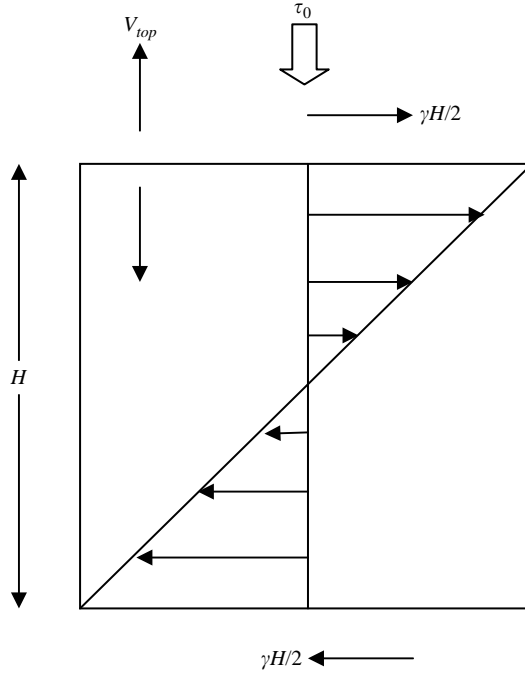


FIGURE 1. A schematic of the stress-controlled simulation control volume.

flows internally spanned by force chains that form, rotate and destruct in the shear flow, it is necessary to chose a scheme that maintains the degree of compression in the chain throughout this process. Imagining the force chain as a pole in a pole-vault, this would require the vertical dimension of the control volume to change at a rate proportional to the horizontal velocity (γH) of the upper periodic image. In the spirit of Hoover (1985), the y -direction boundary is moved at a rate $\dot{\chi}H$ proportional to the degree of stress imbalance (i.e. difference between the realized (τ_{yy}) and desired stress levels (τ_0)). However, whereas Hoover used an arbitrary relaxation time, here we have an appropriate flow time scale, the inverse shear rate $1/\gamma$, governing the rate at which stresses change. Compared to molecular systems, granular systems are very stiff and, following the idea discussed above, it was found necessary to limit the rate of boundary movement to γH , roughly reflecting the vertical motion of a rotating force chain,

$$\dot{\chi} = \min \left\{ \gamma \frac{\tau_{yy} - \tau_0}{\tau_0}, \gamma \frac{\tau_{yy} - \tau_0}{|\tau_{yy} - \tau_0|} \right\}. \quad (3.2)$$

Furthermore, to maintain the periodic structure, each particle is moved along with the boundary at a rate appropriate to its position so that the entire system expands and contracts as a whole. Thus, as the top moves with velocity $\dot{\chi}H$, a particle with its centre at a vertical coordinate y moves with vertical velocity $\dot{\chi}y$. With this scheme, the averaged stress is equal to the desired stress to within 1%. In nearly all cases, the normalized r.m.s. density variation ($\sqrt{\langle (v - \langle v \rangle)^2 \rangle} / \langle v \rangle$, where $\langle \rangle$ represents a time average) was in most cases less than 0.5%, and in more than half the cases, less than 0.25% indicating the extremely small density changes required to maintain the applied stress. (Only 5 out of the 242 simulations used for this study, all for $\mu = 0.1$, had r.m.s. concentration fluctuations exceeding 1% and all were less than 2%.)

For the initial state of the system, the particles are positioned randomly within the cell with velocities appropriate to their position in the shear flow. To produce a random initial configuration at large solids concentrations, the particles were inserted at random positions but at half their desired radius (i.e. at an initially small concentration). Then the shear flow was set in motion and during the initialization stage of the simulation, the particles were grown to their final diameters. During this time, the shear flow is allowed to distribute them as it will, so that the particle configuration is eventually determined by the concentration and by the necessity of conforming to a shear flow. This technique was chosen after considering many other possible ways of initializing the system; see Campbell (2002) for details. Note that at the concentrations of interest in this paper and because the material is shearing, the material cannot form crystal structures. Tests reported in Campbell (2002) indicate that even if started in regular crystal-like packings, the system will eventually break out of the regular structure and demonstrate the same rheological behaviour as the random systems studied here.

When the bulk granular material is responding elastically to the applied forces, the Young's modulus of the bulk material is proportional to the stiffness k (for systems of particles, the relationship was derived by Bathurst & Rothenburg 1988). The stiffness between real solid particles is strongly dependent on the geometry of, and pressure on, the contact and is thus not solely determined by the elastic moduli of the solid material that makes up the particles. As a result, k and not the elastic properties of the constituent solid, is the important parameter in determining the elastic behaviour of the bulk granular material. Linear contacts are used here because they have only a single constant k that may be used as a scaling parameter. For the same reason, only monodisperse spheres are studied as that allows the particle diameter d to be used as a well-defined intrinsic length scale. These assumptions dictate that any binary collision between particles will have a fixed contact time regardless of the velocity or other properties of the impact:

$$T_{bc} = \frac{\pi}{\sqrt{\frac{2k}{m} - \frac{D^2}{m^2}}}. \quad (3.3)$$

As in Campbell (1993c, 2002) and Potapov & Campbell (1996), the value of the average actual contact time relative to T_{bc} may be used as an indicator of whether the material is behaving in a collisional (rapid flow) or elastic manner.

4. Interpretation of the governing dimensionless parameters

The parameters that govern the stress are:

$$\tau = f(v, k, \gamma, d, \rho, \mu, D). \quad (4.1)$$

Here, τ is the stress, v is the solid concentration, d is the diameter, ρ is the density of the solid material that makes up the particles, and μ is the particle surface friction. In this case, τ is fixed by the applied stress τ_0 so the free parameter is the average concentration \bar{v} so that:

$$\bar{v} = f\left(\frac{\tau_0 d}{k}, \frac{k}{\rho d^3 \gamma^2}, \mu, \epsilon\right). \quad (4.2)$$

Tests show that this scaling is very robust. In fact, many of the data sets in this paper have at least two virtually indistinguishable overlapping data points, i.e. points with

the same $\tau d/k$ and $k/(\rho d^3 \gamma^2)$, but using different τ , k and γ . (More extensive tests were performed in Campbell 2002, with as many as 9 indistinguishable overlapping points in the figures.)

As pointed out in Campbell (2002), $\tau d/k$ may be thought of as the deformation induced in a particle by the stress τ scaled by the particle diameter. The elastic parameter $k/(\rho d^3 \gamma^2)$ was given three interpretations. Probably the most useful is to think of $(k/(\rho d^3 \gamma^2))^{-1/2}$ as the fraction of a particle diameter that a particle will deform owing solely to the inertia of the particle impact. However, since generally $2km \gg D^2/m^2$ in (3.3) (unless the coefficient of restitution ϵ is very small), the parameter may be interpreted as the squared ratio of the flow time scale ($1/\gamma$) to the binary collision time, T_{bc} . Thus, at small values of $k/(\rho d^3 \gamma^2)$, the shear rate γ is pushing particles together, generating contacts at a rate comparable to the rate at which the elastic contact forces push them apart; this accounts for Campbell's (2002) observation that, at small $k/(\rho d^3 \gamma^2)$, force chains can form at surprisingly small concentrations and cause a transition from inertial to elastic behaviour.

In stress-controlled systems, it is not possible to determine the flow regime from direct examination of the stress behaviour as all the components of stress vary proportionally to the applied stress. Thus, changing the shear rate or concentration at a fixed applied stress will have little effect on the magnitude of the other stress components. Because the stress behaviour cannot be used, it is necessary to find indirect ways of determining the flow regime. One indicator of the elastic–quasi-static \leftrightarrow elastic–inertial transition, can be found from the concentration ν ; when ν becomes dependent on $k/(\rho d^3 \gamma^2)$, the flow is dependent on the shear rate and has thus transitioned to elastic–inertial behaviour. But while that particular determination may only be made in stress-controlled flows, other methods of flow-regime determination are already apparent in the fixed-concentration results of Campbell (2002). For example, it was observed that in the elastic–inertial regime, the stress ratio τ_{xy}/τ_{yy} , decreases with $k/(\rho d^3 \gamma^2)$ and becomes constant when the flow transitions to elastic–quasi-static behaviour; this change will be used as another indicator of the elastic–quasi-static \leftrightarrow elastic–inertial transition. An indicator of the elastic–inertial \leftrightarrow inertial transition can be found from the ratio t_c/T_{bc} , of the actual collision time t_c to the binary collision time T_{bc} given in (3.3). Any binary collision must, within numerical precision, occur in T_{bc} and can only be extended if there are simultaneous interactions between three or more particles. If the particles are locked in force chains as in the elastic–quasi-static and elastic–inertial regimes, then the actual contact time is roughly the same as the lifetime of the chain. The chain's life is a process of (i) formation as the shear flow drives the particles together, (ii) rotation of the chain in the shear flow, and (iii) eventual destruction as the rotation makes the chain unstable. All of these processes are controlled by the shear rate, and Campbell (2002) demonstrated that in the elastic–quasi-static and elastic–inertial regimes, t_c/T_{bc} varies as a function of $k/(\rho d^3 \gamma^2)$ and should be roughly inversely proportional to the shear rate. Campbell (2003) found that for a contact to endure for such long periods of time (up to a thousand T_{bc}), it must be locked in a force chain that is loaded at a value comparable to the force on the contact. Such a force must be applied external to the chain, for example by bounding walls; as there are no walls in the simulation to apply such a force, this requires that the force chains close on themselves across the periodic boundaries so that, in effect, the chains are infinitely long. When t_c/T_{bc} increases with $k/(\rho d^3 \gamma^2)$, the flow is elastic (i.e. either elastic–quasi-static or elastic–inertial) and when independent of $k/(\rho d^3 \gamma^2)$, the flow is inertial.

Figure 2 shows snapshots of the contact forces inside the control volume for cases that, by the above prescriptions, correspond to the elastic–quasi-static, elastic–inertial and collisional regimes, respectively. As this is a three-dimensional system, these pictures represent projections of the contact forces onto the various planes. In each subfigure, the large figure on the left-hand side represents the projection onto the shear plane (x, y -plane). (Here the mean flow is in the x -direction and the velocity gradient is in the y -direction.) The smaller inserts on the right-hand side represent the projections onto the x, z -plane (top) and the y, z -plane (bottom). By using all three projections, it is possible to follow the paths of force chains through the control volume. Following a long tradition originating with Cundall & Strack (1979), each line goes between the centres of contacting particles and the width of the line represents the force. The scale varies in each subfigure. In the large shearplane figure, the largest stress is represented by a line 15 times thicker than the smallest. (For clarity, in the smaller subfigures on the right-hand side, the largest stress lines are only 7 times thicker than the smallest.) A complicated contact network of force chains is plainly apparent in figures 2(a)–2(c), representing the elastic–quasi-static and elastic–inertial regimes. In the collisional regime, figure 2(d), the contact lines appear infrequently and are only a single particle diameter long. figures 2(b) and 2(c) both lie in the elastic–inertial, figure 2(b) lies near the elastic–quasi-static/elastic–inertial transition and figure 2(c) lies near the elastic–inertial/collisional transition. Other than that, these figures were chosen more or less at random from the more than 200 simulations used in this study and each represents the contact network that existed at the end of the simulation. Notice that the elastic–inertial figure 2(b) is nearly indistinguishable from the elastic–quasi-static case in figure 2(a) showing that the transition is only due to inertial effects and not due to changes in the internal structure (although, as the structure is unsteady, we should not draw too many conclusions from snapshots). This may be somewhat surprising as the concentration for figure 2(b) ($\nu = 0.57$) is smaller than that for figure 2(a) ($\nu = 0.59$), so that this is indicative of the ability of shear to generate force chains.

For simplicity, the shorthands, $T^* = \tau_0 d/k$ and $k^* = k/(\rho d^3 \gamma^2)$ will occasionally be used, especially in figure legends where space is at a premium.

4.1. Appropriate values for the dimensionless confining stress, $\tau_0 d/k$

To determine appropriate values of $\tau_0 d/k$, it is first necessary to estimate appropriate values of the interparticle stiffness k . Measurements (Richart, Woods & Hall 1970; Richart 1978) show that the sound speed in loose 1 mm sand is of the order of 100 m s^{-1} which implies that, discarding constants of order 1, $\sqrt{E/\rho} \sim 100 \text{ m s}^{-1}$ where E and ρ are the Young's modulus and density of the bulk sand. Assuming a 60% packing fraction $\rho \sim 1500 \text{ kg m}^{-3}$, making E of the order of $1.5 \times 10^7 \text{ Pa}$. Now Bathurst & Rothenburg (1988) showed that $E \sim nk/d$ where n , is the coordination number (which usually has a value around 3 in a loose medium). Thus, dropping n , as an order 1 constant,

$$k \sim (1.5 \times 10^7 \text{ Pa})(0.001 \text{ m}) = 15\,000(\text{Pa} \cdot \text{m}) = 15\,000 \text{ N m}^{-1}.$$

Now assume that the applied stress τ_0 is exerted by an overburden h , of material, so that $\tau_0 = \rho gh \approx 15000 h \text{ Pa}$. Hence

$$\frac{\tau d}{k} = \frac{(15\,000 h \text{ Pa})d}{15\,000 \text{ N m}^{-1}} = (1 \text{ m}^{-2})hd = (0.001 \text{ m}^{-1})h.$$

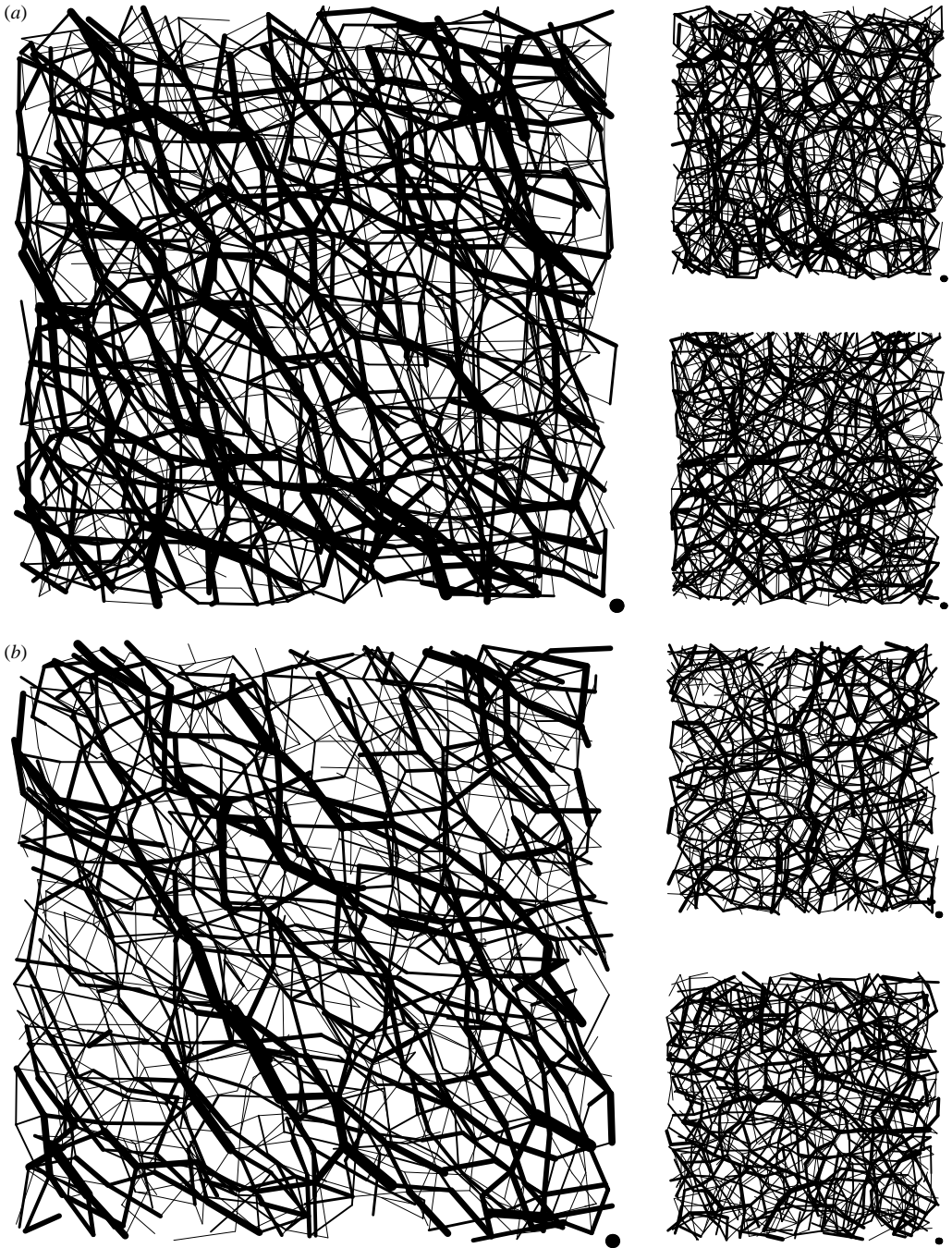


FIGURE 2(a, b). For caption see facing page.

Consequently, an overburden of one particle diameter ($h=0.001$ m) corresponds to $\tau_0 d/k=10^{-6}$, probably the smallest overburden of interest. At the other end of the spectrum, $\tau_0 d/k=10^{-1}$ corresponds to a 100 m overburden (and a 10% mean particle deformation); while even deeper flows might be possible, particularly in large landslides, such a large stress would undoubtedly crush and grind brittle particles

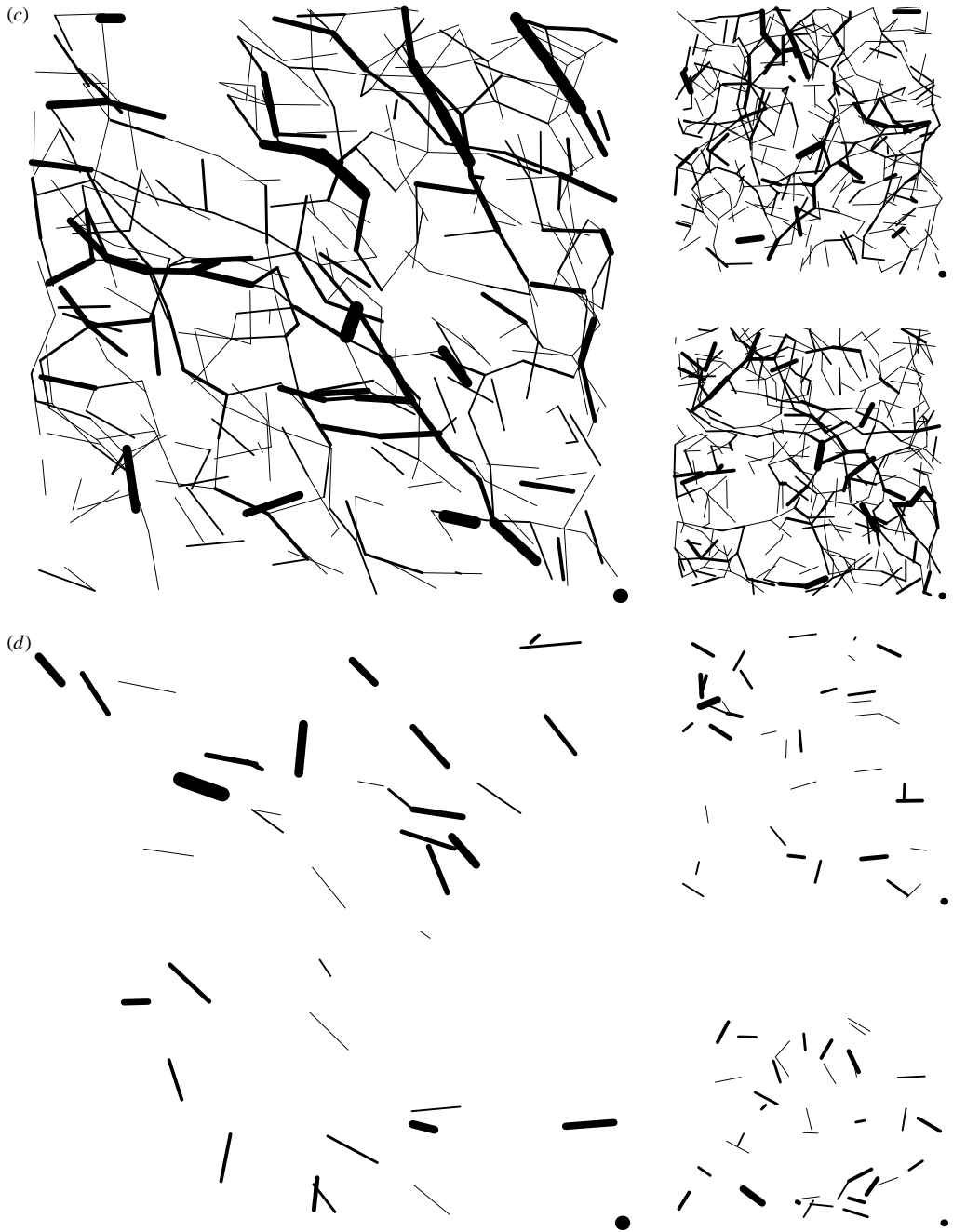


FIGURE 2. Snapshots of the contact force network. The large figure to the left-hand side is the projection in the (x, y) -plane. The top figure on the right-hand side is the projection onto the (x, z) -plane and the bottom is the projection onto the (y, z) -plane. Each line connects the centres of the contacting particles with a width proportional to the force on the contact. (a) Elastic-quasi-static, $\tau_0 d/k = 10^{-3}$, $k/(\rho d^3 \gamma^2) = 10^7$, $\nu = 0.59$, (b) elastic-inertial $\tau_0 d/k = 5 \times 10^{-4}$, $k/(\rho d^3 \gamma^2) = 10^6$, $\nu = 0.57$, (c) elastic-inertial $\tau_0 d/k = 2 \times 10^{-5}$, $k/(\rho d^3 \gamma^2) = 10^6$, $\nu = 0.55$, and (d) collisional $\tau_0 d/k = 10^{-5}$, $k/(\rho d^3 \gamma^2) = 10^5$, $\nu = 0.45$. For all, $\mu = 0.5$.

(which, of course, happens frequently). While there are some granules (golf, tennis and most other sports balls, for example) that can easily respond elastically to even 50 % deformations, $\tau_0 d/k = 10^{-1}$ is a reasonable upper bound for this study (especially as going another order of magnitude to $\tau_0 d/k = 10^0$, implies a 100 % overlap). Consequently, this paper will vary $\tau_0 d/k$ within the range 10^{-6} to 10^{-1} .

It should also be noted that there is a minimum value of $\tau_0 d/k$ that is achievable in the simulation for each value of $k/(\rho d^3 \gamma^2)$. This is evident from rapid flow theory where the stresses are singular both as ν approaches the shearable limit and as $\nu \rightarrow 0$ (i.e. $\tau \rightarrow \infty$ at the shearable limit and as $\nu \rightarrow 0$, see for example, Lun *et al.* 1984; Campbell 1989, 1990). In between, the scaled stress, $\tau/(\rho d^2 \gamma^2)$ reaches a minimum value whose magnitude and location depends on the coefficient of restitution ϵ , and the surface friction μ (this usually occurs around $\nu = 0.2$ and thus far below the concentrations of interest in this paper). If a smaller value of $\tau_0 d/k = \tau_0/(\rho d^2 \gamma^2)/(k/(\rho d^3 \gamma^2))$ is specified, it is impossible for the system to reach a force balance. Thus, for small $\tau_0 d/k$, the achievable values of $k/(\rho d^3 \gamma^2)$ are restricted, e.g. at $\tau_0 d/k = 10^{-6}$, the smallest accessible shear rate corresponds to $k/(\rho d^3 \gamma^2) = 10^6$.

5. Results

For given material properties, once the applied stress and shear rate are specified, (fixing $\tau_0 d/k$ and $k/(\rho d^3 \gamma^2)$), (4.2) dictates that the only dependent parameter is the solid fraction ν which will itself vary slightly over time as the control volume expands and contracts. We can anticipate three regimes of behaviour for ν as a function of $\tau_0 d/k$ and $k/(\rho d^3 \gamma^2)$. At very large loadings, the bulk material will be compressible because of the compressibility of the contacts. For example, the 10 % deformations expected at $\tau_0 d/k = 10^{-1}$ means that the particle centres are 10 % closer than a particle diameter, resulting in a 37 % increase in concentration. However, we can expect that as the burden is relaxed, there will be little dependence of ν upon $\tau_0 d/k$ at small shear rates, simply because the particle deformations become insignificant; in other words, there will be no significant concentration difference between the 0.1 % particle deformations of $\tau_0 d/k = 10^{-3}$ and the 0.001 % deformations of $\tau_0 d/k = 10^{-6}$.

This last is characteristic of ‘critical state’ behaviour (see for example Casagrande 1938; Roscoe *et al.* 1958; Schofield & Wroth 1968). Slowly shearing a granular material will either dilate or consolidate as needed until it assumes a fixed ‘critical state’ concentration, whose value is a function of the material type and the applied load. The variation of the critical state concentration with load is due to particle compressibility and at small loads becomes independent of loading as the compressibility becomes insignificant. The term ‘low-stress critical state concentration’ will be used to refer to this small-load limit in the following figures.

Finally, when the shear rate becomes large, the applied stress can be supported by the inertia of the particles and the flow will deviate from the low-stress critical state behaviour.

Figure 3 shows the time-averaged values of ν as a function of $\tau_0 d/k$, for various values of $k/(\rho d^3 \gamma^2)$ and three values of the particle surface friction $\mu = 0.1, 0.5, 1.0$. All three regimes mentioned above: particle compressibility, critical state and inertial deviation are apparent in this figure. Naturally, the larger the shear rate (the smaller the $k/(\rho d^3 \gamma^2)$), the larger the applied stress at which the curve deviates from the critical state.

As these observations concern only the concentration and not the stress–strain behaviour, they cannot be directly related to the elastic–quasi-static, elastic–inertial

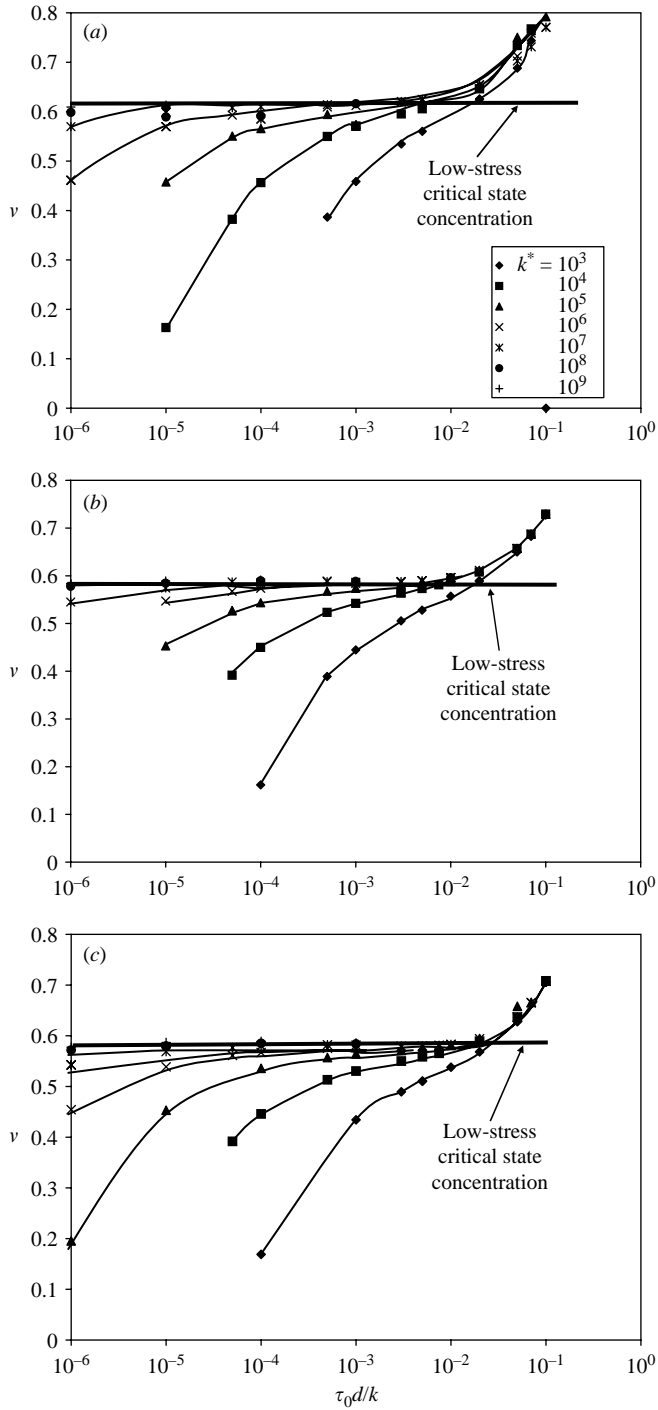


FIGURE 3. The variation of the the solids concentration v with the dimensionless applied stress, $\tau_0 d/k$ for various values of $k/(\rho d^3 \gamma^2)$: (a) $\mu = 0.1$, (b) $\mu = 0.5$ (c) $\mu = 1.0$. The deviation from the critical state concentration line is used as an indicator of the elastic–quasi-static to elastic–inertial transition. Here $k^* = k/(\rho d^3 \gamma^2)$.

and inertial regimes. However, the points where the lines for the various $k/(\rho d^3 \gamma^2)$ deviate from the critical state can be considered the first appearance of inertial effects and are potential indicators of the elastic–quasi-static/elastic–inertial transition. (A similar plot can be found in Aharonov & Sparks (1999) although they identified this as a ‘solid’ to ‘gas’ transition despite evidence of force chains in some of the ‘gas’ states. They also showed that the stress power spectral density had a slope near unity in the elastic–inertial regime which might reflect the linear dependence of the stresses on the shear rate.)

The ‘low stress critical state lines’ shown in figure 3 are simply drawn by eye through the small shear rate (large $k/(\rho d^3 \gamma^2)$) points. Note that the data for the various $k/(\rho d^3 \gamma^2)$ congregates about these lines until they diverge one by one, with the smallest $k/(\rho d^3 \gamma^2)$ (largest shear rate) diverging at the largest $\tau_0 d/k$. Notice that the critical state values for $\mu = 0.5$ and $\mu = 1.0$ are at $\nu = 0.58$, while the $\mu = 0.1$ line is somewhat higher at about $\nu = 0.61$. These values coincide with the elastic–quasi-static \leftrightarrow inertial transition points observed at fixed concentration and large $k/(\rho d^3 \gamma^2)$ by Campbell (2002). As in Campbell (2002), the larger critical concentration for $\mu = 0.1$ can be attributed to a weakening of the force chains by the small surface friction.

Figure 4 shows the corresponding cases for the stress ratio, τ_{xy}/τ_{yy} as a function of $k/(\rho d^3 \gamma^2)$. To avoid cluttering the figure with too much data, only the lines for the decade values of $\tau_0 d/k$ are shown. As with the constant volume studies in Campbell (2002), τ_{xy}/τ_{yy} initially falls as $k/(\rho d^3 \gamma^2)$ increases, demonstrating elastic–inertial behaviour, and becomes constant at large $k/(\rho d^3 \gamma^2)$, demonstrating elastic–quasi-static behaviour. (This transition was used to first identify the two flow regimes in Campbell 2002.) Thus, the intersection of the sloping and horizontal lines will be used as a second indicator of the elastic–inertial and elastic–quasi-static regimes. In interpreting this figure, the reader should remember that the concentration is not constant along each of the lines and is generally decreasing as we move from right to left in the figure. This might explain some of the features of these plots. For the fixed-concentration studies (Campbell 2002) the transition between the elastic–inertial and elastic–quasi-static regimes was a relatively abrupt change from a steeply sloping line and a flat $\tau_{xy}/\tau_{yy} = \text{const}$ line. Here, many of the curves demonstrate a longer and more gently sloping transitional stage before attaining quasi-static behaviour. In fact, the highest applied stress cases never show the more steeply sloping behaviour; consequently, these highest stress lines are not used to distinguish the flow-regime transitions.

Particle surface friction can be seen to have an effect both on the overall value of the stress ratio τ_{xy}/τ_{yy} , and on the limiting quasi-static value as $k/(\rho d^3 \gamma^2) \rightarrow \infty$. Notice that the largest values of τ_{xy}/τ_{yy} can reach 0.8 for $\mu = 0.5$ and $\mu = 1.0$, but do not exceed 0.6 for $\mu = 0.1$. Furthermore, the limiting quasi-static values of τ_{xy}/τ_{yy} decrease only slightly going from $\mu = 1.0$ to $\mu = 0.5$, but are significantly smaller for $\mu = 0.1$. Much the same behaviour was observed in the fixed-concentration results of Campbell (2002), although the limiting value of the $\mu = 0.1$ data is slightly smaller here. There is also some odd behaviour for the higher stress levels in the low friction, $\mu = 0.1$, data in figure 4(a). Note that for small values of $k/(\rho d^3 \gamma^2)$, and $\tau_0 d/k = 0.01$ and 0.1, the stress ratio τ_{xy}/τ_{yy} falls below the eventual quasi-static limit. This may be explained by first noting that such small friction allows the particle surfaces to readily slip relative to one another. If the particle surfaces do not frictionally lock together, then the system does not go through the process of force chain formation, rotation and disintegration. Instead, the shear stress is largely generated by the geometric constraint that the particles have to pass around one another to maintain

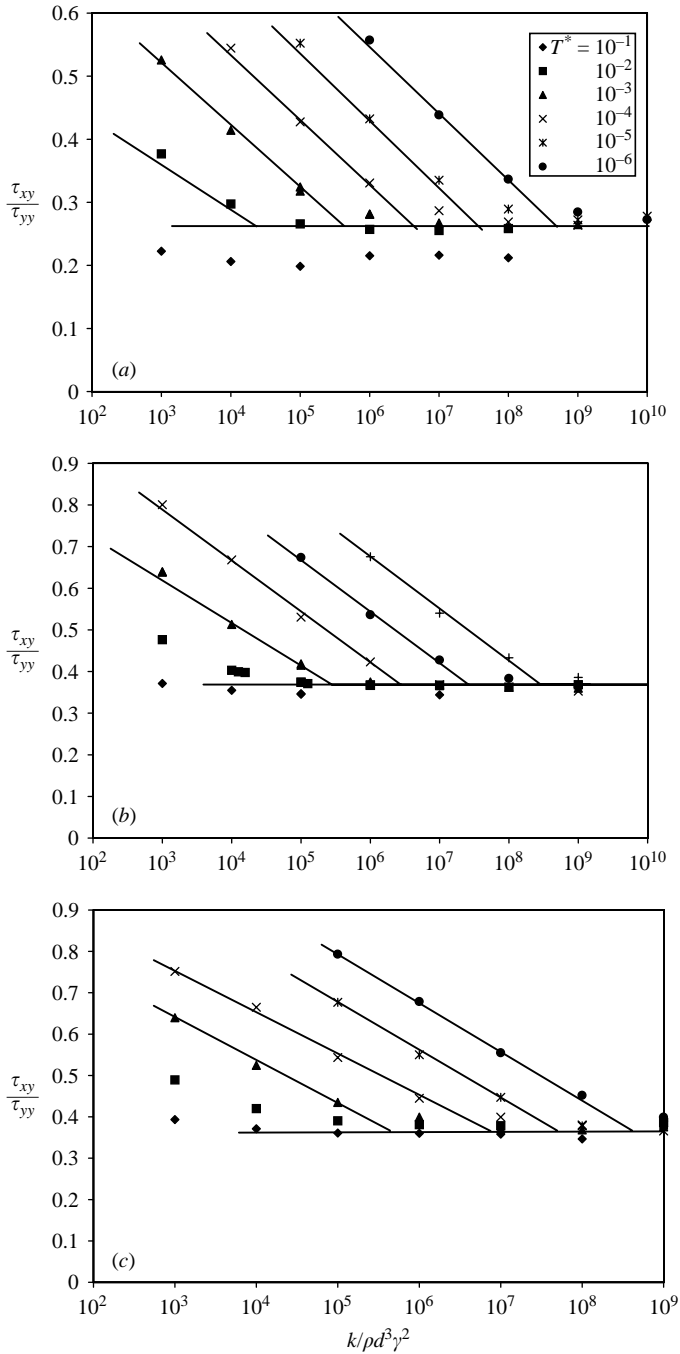


FIGURE 4. The stress ratio, τ_{xy}/τ_{yy} as a function of $k/(\rho d^3 \gamma^2)$ for various $\tau_0 d/k$: (a) $\mu = 0.1$, (b) $\mu = 0.5$ (c) $\mu = 1.0$. The intersection of the steeply sloping and horizontal lines in figure 3 is used as an indicator of the elastic–quasi-static to elastic–inertial transition. Here $T^* = \tau_0 d/k$.

a shear flow. At high stress levels, the particles are highly deformed and it is possible their surfaces simply squeeze through the constraint producing smaller shear stresses. (A similar behaviour was seen for very soft particles by Zhang & Campbell 1992).

How can we detect the transition from elastic–inertial to inertial (either non-collisional or collisional) behaviour? Once again, the magnitudes of the stresses are dictated by the applied stress and only indirect indications are possible; but remember that the physical nature of elastic–inertial behaviour is that (i) the particles are locked into force chains, as in elastic–quasi-static behaviour, and (ii) that the inertia is large enough to be reflected in the forces that load the chains. The second criterion can be determined when τ_{xy}/τ_{yy} deviates from quasi-static behaviour as described above. Also as mentioned above, the existence of force chains can be deduced from the contact time ratio t_c/T_{bc} . In true rapid granular flows, all particle interactions are collisional and $t_c/T_{bc} = 1$. In elastic flows, where the particles become trapped in force chains, the interparticle contact time is roughly the life of the chain and thus depends on γ and is independent of T_{bc} ; thus t_c/T_{bc} will be a function of $k/(\rho d^3 \gamma^2)$ and will have a slope near 1/2 when plotted on a log–log plot.

Such a plot is shown in figure 5. Note that there is generally a sharp transition between inertial–collisional ($t_c/T_{bc} = 1$) and elastic behaviour ($t_c/T_{bc} = f(k/(\rho d^3 \gamma^2))$ with slope near 1/2). There is little evidence of the intervening inertial–non-collisional regime in which $t_c/T_{bc} > 1$ (indicating simultaneous interactions of more than two particles), but with no apparent power-law dependence on $k/(\rho d^3 \gamma^2)$ even though that regime was prominent in the fixed-concentration studies. For these controlled stress cases, it appears that either the particles interact by binary collisions, or they deviate onto a line with slope near 1/2, with only at most one or two points between that indicate a transitional behaviour.

Note that the ultimate slope of the t_c/T_{bc} lines appears to be a function of the surface friction coefficient μ . The smallest surface friction, $\mu = 0.1$, is the most complicated. There, the line for the largest applied stress $\tau_0 d/k = 0.1$, exhibits a slope slightly smaller than 1/2, but in the intermediate range, the slope is equal to 1/2, becoming larger than 1/2 for the smallest $\tau_0 d/k$. For the larger values of the friction coefficient, $\mu = 0.5$ and $\mu = 1.0$, a nearly opposite behaviour is observed. For the largest applied stress, $\tau_0 d/k = 0.1$, the slopes equal 1/2, but smaller slopes are observed for smaller values $\tau_0 d/k$. There is also no increase in slope for the smallest $\tau_0 d/k$ as seen for $\mu = 0.1$. The reasons for this are not clear. Remember, however, (i) that the system will expand if the stresses become too large and (ii) that the larger the friction coefficient μ , the larger the force that can be supported by the force chains. Thus, it appears that for the larger μ the system expands to relax the stress and allows the chain to break apart early; but at the largest loadings the chains are held tightly together, cannot break early and thus produce a slope of 1/2. While those arguments would seem to account for most aspects of the observations, this behaviour is not well understood.

Collectively, these ideas can be used to create the flowmaps in figure 6, indicating the flow regimes as functions of $k/(\rho d^3 \gamma^2)$ and $\tau_0 d/k$. The transition from elastic–quasi-static to elastic–inertial behaviour is determined in two ways: (i) the deviation from critical state behaviour in figure 3, and (ii) the transition apparent in the τ_{xy}/τ_{yy} plots in figure 4. As shown in figure 4, the transition point is taken to be the intersection between a line drawn through the steeply sloping portion of the curve and one through the quasi-static portion. The transition from elastic–inertial to inertial–collisional behaviour is determined by drawing a line through the sloping points in the t_c/T_{bc} curves in figure 5 and seeing where it intersects the $t_c/T_{bc} = 1$ line. Because this technique essentially extrapolates the point where $t_c/T_{bc} = 1$, it predicts the onset of not just inertial behaviour, but true collisional (rapid flow) behaviour. The transition points are enclosed by shaded boundaries because these techniques are somewhat *ad hoc* and imprecise.

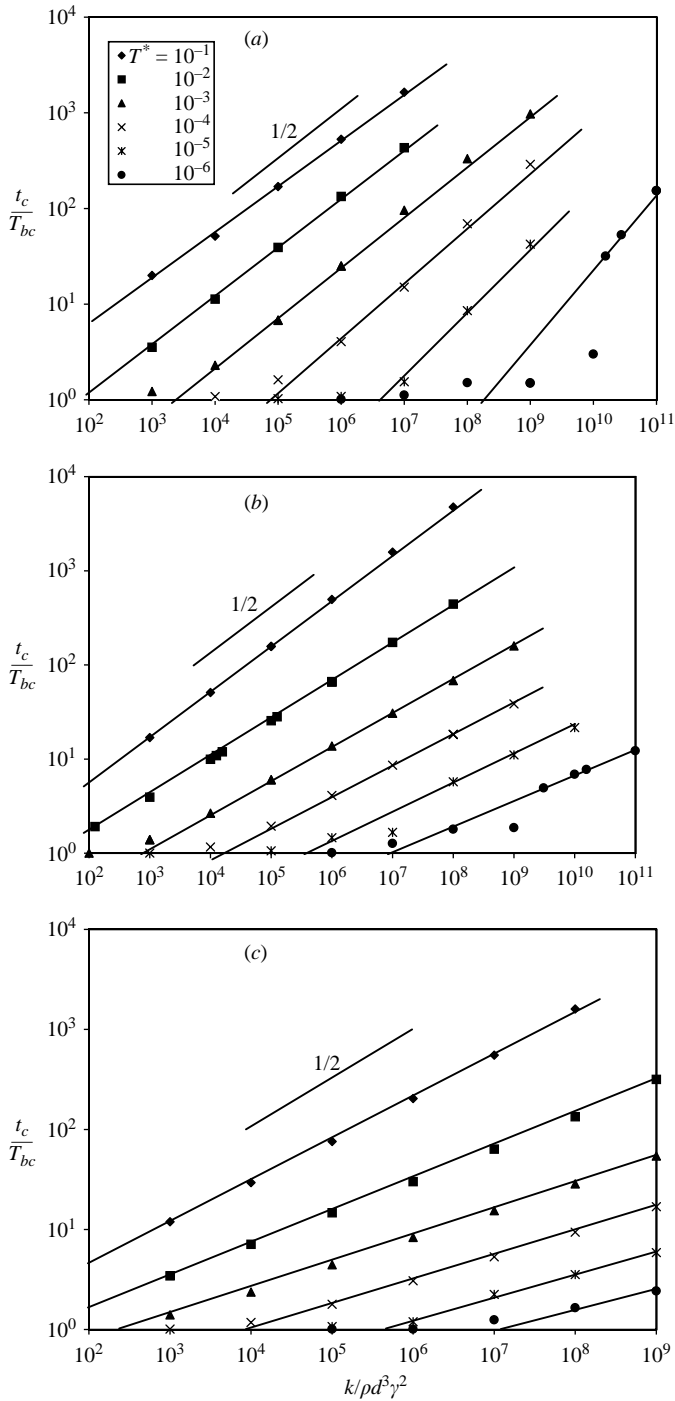


FIGURE 5. The ratio of the contact time to binary collision time, t_c/T_{bc} as a function of $k/(\rho d^3 \gamma^2)$ for various $\tau_0 d/k$: (a) $\mu = 0.1$, (b) $\mu = 0.5$, (c) $\mu = 1.0$. The intersection of the sloping and $t_c/T_{bc} = 1$ lines is used as an indicator of the elastic–inertial to inertial–collisional transition. Here $T^* = \tau_0 d/k$.

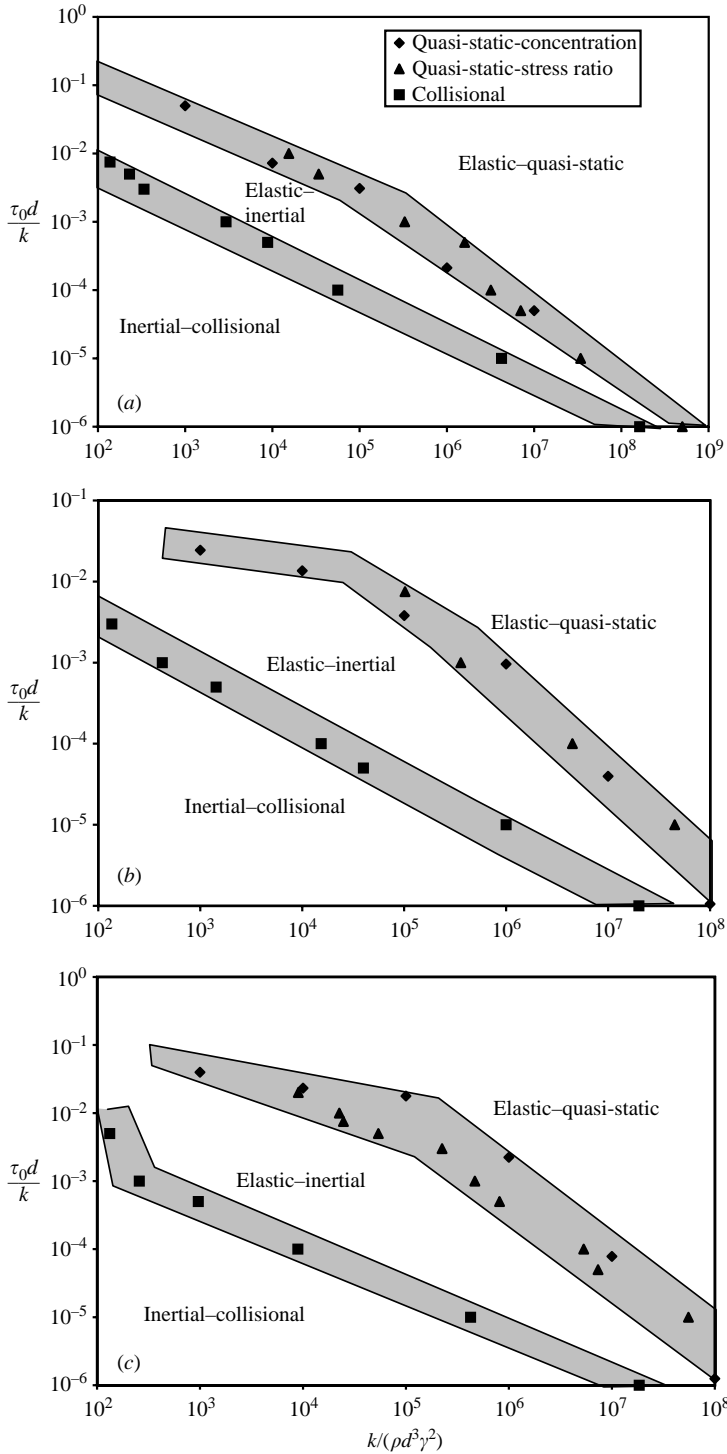


FIGURE 6. Flowmaps showing the parametric boundaries for the elastic–quasi-static, elastic–inertial and inertial–collisional flow regimes. The elastic–quasi-static to elastic–inertial boundary is determined in two ways (i) by the appearance of inertial effects in the concentration data in figure 2 (the quasi-static-concentration points) and (ii) by the line intersections in the stress ratio data of figure 2 (the quasi-static-stress ratio points). The elastic–inertial to collisional transition is determined from the t_c/T_{bc} data in figure 4.

The nearly direct transition from elastic–inertial to inertial–collisional behaviour should be expected as little of the inertial–non-collisional regime is apparent in figure 5. In other words, there are few points that do not fit either on the $t_c/T_{bc} = 1$ line or on one of the sloping lines and could be considered to be transitional between collisional and elastic behaviour. Until the inertia of the particles is sufficient to support the applied load, some of the load will have to be supported elastically, holding the particles together in force chains. When inertia can support the load, the particles do not have to remain in persistent contact and the flow dilates so that the particles lose contact with their neighbours and interact collisionally. In fixed concentration flows, however, the system is not free to expand and may be maintained at a concentration where simultaneous multiparticle contacts are possible, but, as there is no applied load, such structures will break apart with time scales of the order of the binary collision time.

6. Discussion

The flow maps in figure 6 intuitively seem much more reasonable than the corresponding fixed concentration results in Campbell (2002). Notice that at a fixed loading, $\tau_0 d/k$, increasing the shear rate γ (decreasing $k/(\rho d^3 \gamma^2)$), causes a transition from elastic–quasi-static \rightarrow elastic–inertial \rightarrow inertial–collisional behaviour, just as we would intuitively expect. At fixed concentration, the results were surprisingly different. First of all, only transitions between elastic–quasi-static \leftrightarrow elastic–inertial or elastic–inertial \leftrightarrow inertial (collisional or non-collisional) behaviours were observed at fixed concentration; there was no path between elastic–quasi-static and inertial behaviour except by reducing the concentration. (This is easily understood because, at large concentrations, the particles must stay in contact with their neighbours, i.e. are locked in force chains regardless of the shear rate.) An even stranger aspect of fixed-concentration flows was that elastic–inertial \rightarrow inertial–non-collisional \rightarrow inertial–collisional (rapid-flow) transition is accomplished by increasing $k/(\rho d^3 \gamma^2)$, which can be brought about by reducing the shear rate, thus leading to the conclusion that ‘rapid flows’ are less rapid than non-rapid flows (although this makes more sense if we think of the $k/(\rho d^3 \gamma^2) \rightarrow \infty$ limit as the $k \rightarrow \infty$ limit, rather than the $\gamma \rightarrow 0$ limit, implying rigid particles and collisional interactions). The opposite behaviour is observed in these stress-controlled flows. This is the first indication that these types of system-scale constraints affect the rheology and suggests that the results of controlled-stress flows cannot be applied to constant-volume flows and vice versa.

The fact that rapid flows now appear at small $k/(\rho d^3 \gamma^2)$ in controlled stress flows, presents its own set of conceptual difficulties. Small $k/(\rho d^3 \gamma^2)$ corresponds to the large shear rate limit where we would expect rapid flows, but it also corresponds to a small k limit, indicating soft particles. This may at first appear surprising as rapid flow theory assumes instantaneous collisions which imply the $k \rightarrow \infty$ limit. However, in the controlled stress case, the apparent contradiction is something of an illusion as k also appears in the vertical ordinate $\tau_0 d/k$. Thus, reducing k with all other dimensional quantities fixed, moves us diagonally on the flowmap into regions of higher stress and thus away from the rapid-flow regime. Alternatively, moving horizontally by reducing k at constant $\tau_0 d/k$, requires reducing τ_0 so that τ_0/k remains a constant, thus entering the rapid-flow regime by reducing the stress instead of increasing the shear rate.

These flowmaps give an indication of why rapid granular flows are seldom observed under Earth’s gravity. For example, these results predict that a flow of

$\mu = 0.5$ spheres becomes collisional at about $\tau_0 d/k = 10^{-5}$ (which for the 1 mm sand used as an example in §4.1, corresponds to a flow of about 10 particles deep) and $k/(\rho d^3 \gamma^2) = 10^6$. Continuing the use of the sand numbers from §4.1, this corresponds to a shear rate of about 100 s^{-1} , which is in the same range as the minimum values reported by Wang & Campbell (1992) for 3 mm glass spheres on systems of similar depth. The Wang & Campbell results show that the minimum shear rate decreased with particle size in roughly the same way as predicted by these results. For a fixed stress, inertial flows appear at a fixed $k/(\rho d^3 \gamma^2)$. Now, measurements by Hostler & Brennen (2003) indicate that the soundspeed in spherical particles is independent of their diameter. According to Bathurst & Rothenberg (1988) this fixes $k/(\rho d)$. Then the minimum inertial shear rate should vary so that $d\gamma_{min} = \text{const}$, which the preceding order of magnitude calculations suggest is of the order of $d\gamma_{min} = 0.1 \text{ m s}^{-1}$. The largest concentration ($\nu = 0.5$) Wang & Campbell results show that for 1.9 mm glassbeads, $d\gamma_{min} = 0.34 \text{ m s}^{-1}$, for 3.0 mm glassbeads, $d\gamma_{min} = 0.36 \text{ m s}^{-1}$, and for 3.75 mm glassbeads, $d\gamma_{min} = 0.33 \text{ m s}^{-1}$. It should be noted that the Wang & Campbell studies were not attempts to measure the limits of rapid granular flows. However, at shear rates smaller than these, they found the flow was unsteady in a manner that, in light of these results, can be understood as a signal of a regime transition. Wang & Campbell did however, make every attempt to record data at the smallest possible shear rate that did not demonstrate such an instability. Thus, to some extent, these results are anecdotal, but they are still compelling since they found $d\gamma_{min} = \text{const}$ and of the expected order. Also it should be noted that the Wang & Campbell shear cell had roughened walls, while there are no boundaries in these simulations; this may contribute to the quantitative discrepancies noted above.

As mentioned in Campbell (2002), these studies were undertaken to better understand work on landslides (Campbell, Cleary & Hopkins 1995), hoppers (Potapov & Campbell 1996) and the ‘phase-change’ between fluid and solid behaviour (Campbell & Zhang 1992; Campbell 1993c; Zhang & Campbell 1992). All of these indicated that the stress ratio τ_{xy}/τ_{yy} decreased with the shear rate, just as it is observed to do in the elastic–inertial regime. However, the fixed concentration data in Campbell (2002) also indicated that only the landslide data could be so explained; for example, at $\nu = 0.6$, elastic–inertial behaviour was observed for $k/(\rho d^3 \gamma^2) < 10^4$ which for 1 mm sand required about 1000 s^{-1} of shear. (This is much too large for the hopper or phase change studies and only applies to the landslide data because very soft particles were used in the landslide simulations). However, that is not so for the stress-controlled studies shown here. For example, figure 6 indicates that for $\mu = 0.5$ and $\tau_0 d/k = 10^{-5}$ (ten particles deep), elastic–inertial behaviour can first be observed for $k/(\rho d^3 \gamma^2) \approx 5 \times 10^7$ or about $\gamma = 14 \text{ s}^{-1}$. The reason for this is obvious from the underlying physics. Elastic–inertial behaviour occurs when the inertial forces are of the same order as the elastic forces. In the fixed-concentration flows of Campbell (2002), the elastic forces were dictated by the requirement that the particles undergo shear at the large concentrations where force chains form. Reducing the concentration to the point that the force chains disappeared, the elastic forces went away and the stresses dropped by orders of magnitude; this is possible because the concentration was independent of the stresses generated. In constant-stress flows, as long as the shear rate is small enough, force chains can always form even for very small applied stresses, simply because if the inertia effects are small, force chains are the only method available to balance the applied load. For small applied stresses, the corresponding elastic forces are small and it takes a small shear rate to generate inertial forces that are comparable to the elastic forces, pushing the flow into the elastic–inertial regime.

As a result, elastic–inertial behaviour is much more accessible in controlled stress flows. Furthermore when progressing from elastic–quasi-static to inertial behaviour, the flow must go through an intermediate elastic–inertial regime.

A correspondence between the controlled-stress and fixed-concentration studies can be found in the ‘low-stress critical state’ concentrations shown in figure 3. In these studies, the transition is between quasi-static \leftrightarrow elastic–inertial, which are both dominated by force chains; but the transition occurs at the same concentration as the physically different elastic–quasi-static \leftrightarrow inertial transition concentrations observed at constant volume by Campbell (2002) at large $k/(\rho d^3 \gamma^2)$. This correspondence between the two concentrations was first noted for two-dimensional systems by Aharonov & Sparks (1999), although they described both transitions as between ‘solid’ and ‘gas’ states without realizing that they are two physically distinct transitions.

In the civil engineering field of soil mechanics, the critical concentration (which in that discipline is usually referred to as a ‘critical void ratio’ or one minus the critical concentration) is determined by balancing two competing effects induced by a shearing motion. The first is the necessity of a rigid granular to expand in order to allow the particles to pass over one another. This is balanced by the necessity of the material to support an applied stress which tries to compress the material. (Note that this description implicitly assumes controlled-stress constraints.) The critical concentration is a function of the stress level and, as civil engineers are interested in soils heavily loaded by building weight, critical state values extend up into regions where particle compressibility is important and the particle must of necessity be supported elastically.

Thus, Aharonov & Sparks (1999) err in describing the critical state as a ‘rigidity transition’ between solid and gas-like flows at a fixed concentration. It would be hard to argue that figure 2(b) is significantly less rigid than figure 2(a) despite figure 2(b) being a full 2% below the low-stress critical-state line (similar behaviour can be seen in their own figure 7). In controlled-stress situations, the transition is always from elastic–quasi-static \leftrightarrow elastic–inertial (the transition separating figures 2(a) and 2(b)), force chains dominate on both sides of the transition, and thus this is never a rigidity transition. The concept of a rigidity transition separating elastic and inertial flows applies only to controlled-volume situations, and then only at small shear rates. Campbell (2002) has shown that for large shear rates, it is possible to generate force chains at concentrations well below the critical-state value.

Aharonov & Sparks are correct in identifying the low-stress critical-state line as the smallest concentration that can support force chains and thus support an applied load without inertial assistance. For low stress levels (that do not deform particles sufficiently to significantly affect the concentration) and shear rates too small to provide significant inertial support, the material will assume the smallest possible concentration that can support the applied load (the ‘low-stress critical-state’ concentration), which should roughly correspond to the smallest density that can accommodate force chains. Thus regime transitions occur at the same critical concentration, even though the transition is physically different in controlled-stress (elastic–quasi-static to elastic–inertial) and controlled-volume conditions (elastic–quasi-static to inertial–non-collisional). It should be noted that Aharonov & Sparks (1999) actually found slightly different values for their ‘critical grain volume fraction’ at constant stress and volume conditions. The reason why their two-dimensional results do not show that the two values are equal can be traced to their simulation scheme. They used a control volume bound on top and bottom by surfaces roughened with close-packed disks. It has been known for some time (e.g. Campbell 1993b) that

such a roughening, particularly in two dimensions, behaves almost as a flat wall and provides very weak coupling with the moving particles. As a result, such systems have non-uniform shear rates and concentrations and often exhibit stagnant regions. In fact, animations of the Aharonov & Sparks (1999) simulations demonstrate all of these features and in addition are unsteady. The constant-volume flows, in particular, showed stagnant zones packed against one boundary that filled half the shear zone. As a result, care must be taken in generalizing their results.

The results shown here bring into question many studies that use controlled-stress flows as analogues of fixed-concentration flows. Even rheological shear cells such as those used by Savage & Sayed (1984), Hanes & Inman (1985) and Wang & Campbell (1992), as well as Couette-flow computer simulations (Campbell 1982; Campbell & Brennen 1985; Campbell 1993*a, b*) had movable tops so that the concentration is not fixed, but was determined by a balance between the applied stress and the particle response. At least for the cases in which the author was involved, this was done to assure a good mechanical contact between the granular material and the moving boundaries. The physics as described in Campbell (1982, pp. 39–41) point out that at fixed volume, the large internal dissipation causes the shearing material to migrate away from the driving walls toward the centre of the channel, losing contact with the driving boundaries and ceasing to shear – an inelastic clustering of the type studied by Hopkins & Louge (1991). By requiring the material to balance an applied stress, a good mechanical contact is maintained between the boundaries and the test material, but the concentration is not truly fixed (although it varies only slightly). Yet, the results of these experiments were presented as stress as a function of shear rate and concentration, as if the concentration were truly, and not just approximately, fixed. All of these shear cell results may have to be reconsidered as controlled-stress instead of fixed-concentration studies.

7. Conclusions

This paper has examined the rheology of granular materials in systems that are stress-controlled so that the forces generated internal to the material must balance an externally applied stress. This requires the concentration to vary slightly, often immeasurably, and thus stress-controlled systems may appear to operate at constant volume. However, because the bulk material is stiff, small concentration changes can have a large effect on the stresses generated and thus on the overall rheology. As a result, the behaviour of controlled-stress flows can be very different from fixed-concentration flows. These differences are significant because stress-controlled flows are by far the most common. For example, the weight of the overburden would control the stress at any point in the interior of flows with free surfaces, such as chutes, landslides and hoppers, and the concentration can vary locally to accommodate that stress as required.

The difference in the rheology between controlled-stress and controlled-volume flows can be seen immediately when comparing the controlled stress flowmaps in figure 6 with their fixed concentration counterparts in Campbell (2002). In particular, the fixed-volume flows approach inertial–collisional behaviour as $k/(\rho d^3 \gamma^2) \rightarrow \infty$ (which, in these circumstances, is best thought of as the $k \rightarrow \infty$ or rigid-particle/collisional interaction limit), while controlled-stress flows approach inertial–collisional behaviour at the opposite limit as $k/(\rho d^3 \gamma^2) \rightarrow 0$ (which is then best thought of as the $\gamma \rightarrow \infty$, or high shear-rate limit). A significant consequence of this work is that rheological tests done at fixed concentration may not be applicable to controlled-stress conditions

at the same averaged concentration and vice versa. However, that should already have been evident from the critical-state hypothesis (Casagrande 1938; Schofield & Wroth 1968) which showed that under controlled stress conditions, a granular material could exert a variety of stresses at the same shear rate with no measurable change in concentration. Conversely, at fixed concentration, only a single stress is exerted at each concentration and shear rate.

These differences may partially explain the difficulty in unifying the quasi-static and rapid flow theories. As the plasticity models on which quasi-static flow theory is based are constructed in stress space, they are easier to implement in situations where the boundary conditions are specified in terms of stress (controlled-stress flows). Rapid flow theories are based on kinetic theory ideas in which the concentration appears explicitly through the pair-distribution function, and thus fit more naturally into fixed-concentration flows.

In some ways, it is surprising that elastic properties have been ignored in the modelling of granular materials. After all, they are granular solids and each granule possesses the elastic properties of a normal solid. They are not molecules as assumed in kinetic theory models, nor do they move through dislocations like plastic solids. Thus, elastic properties (which relate the stress state to the strain in the bulk material) did not previously enter into the modelling owing to the basic assumptions of the plasticity and kinetic theory formalisms. As Coulomb friction relates the stresses at yielding, and furthermore because plasticity models are formulated in stress space, elastic strains do not appear directly in quasi-static models. The goal of the quasi-static models is to predict the large plastic flow resulting from the stress state, and, compared to the plastic flow strains, the small elastic strains induced by the stress state are insignificant. There is then no reason to relate the stresses and elastic strains and as a result, the elastic properties do not appear directly in quasi-static analyses. In rapid flows, particles only interact by instantaneous collision and thus implicitly assume infinite elastic moduli so that, again, the elastic properties do not appear in the models. Thus, including the elastic properties in the rheology requires altering or abandoning some of the fundamental notions on which these granular flow theories are based.

Special thanks to Sasha Potapov for his help with the simulation development and to Michel Tanguay for his help with the figures.

REFERENCES

- AHARONOV, E. & SPARKS, D. 1999 Rigidity phase transition in granular packings. *Phys. Rev. E* **60**, 6890–6896.
- BABIC, M., SHEN, H. H. & SHEN, H. T. 1990 The stress tensor in granular shear flows of uniform, deformable disks at high solids concentrations. *J. Fluid Mech.* **219**, 81–118.
- BAGNOLD, R. A. 1954 Experiments on a gravity-free dispersion of large solid particles in a Newtonian fluid under shear. *Proc. R. Soc. Lond. A* **225**, 49–63.
- BATHURST, R. J. & ROTHENBURG, L. 1988 Micromechanical aspects of isotropic granular assemblies with linear contact interactions. *J. Appl. Mech.* **55**, 17–23.
- CAMPBELL, C. S. 1982 *Shear Flows of Granular Materials*. PhD thesis and Rep. E200.7, Division of Engineering and Applied Science, Pasadena, CA, 260pp.
- CAMPBELL, C. S. 1986 Computer simulation of rapid granular flows. *Proc. 10th Natl Congr. of Appl. Mech. Austin Texas*, pp. 327–38, June 1986. ASME, New York.
- CAMPBELL, C. S. 1989 The stress tensor for simple shear flows of a granular material. *J. Fluid Mech.* **203**, 449–473.

- CAMPBELL, C. S. 1990 Rapid granular flows. *Annu. Rev. Fluid Mech.* **22**, 57–92.
- CAMPBELL, C. S. 1993a Boundary interactions for two-dimensional granular flows. Part 1. Flat boundaries, asymmetric stresses and couple stresses. *J. Fluid Mech.* **247**, 111–136.
- CAMPBELL, C. S. 1993b Boundary interactions for two-dimensional granular flow. Part 2. Roughened boundaries. *J. Fluid Mech.* **247**, 137–156.
- CAMPBELL, C. S. 1993c The transition from fluid-like to solid-like behaviour in granular flows. *Powders and Grains* (ed. C. Thornton), vol. 93, pp. 289–294, A. A. Balkema, Rotterdam.
- CAMPBELL, C. S. 1997 Computer Simulation of powder flows. *Powder Technology Handbook*, 2nd edn (K. Gotoh, H. Masuda & K. Higashitani), pp. 777–794. Marcell Dekker, New York.
- CAMPBELL, C. S. 2002 Granular shear flows at the elastic limit. *J. Fluid Mech.* **465**, 261–291.
- CAMPBELL, C. S. 2003 A problem related to the stability of force chains. *Granular Matter* **5**, 129–134.
- CAMPBELL, C. S. 2004a Granular flows and gas fluidization. *Fluidization XI* (ed. U. Arena, R. Chirone, M. Miccio & P. Salatino), pp. 21–36. ECI NY.
- CAMPBELL, C. S. 2004b Granular flows and gas fluidization. *Intl J. Chem. Reaction Engng* **2**, P2. <http://www.bepress.com/ijcre/vol2/P2>.
- CAMPBELL, C. S. 2004c Elastic granular flows. *Intl J. Chem. Reaction Engng* **2**, P2. <http://www.bepress.com/ijcre/vol2/P2>.
- CAMPBELL, C. S. & BRENNEN, C. E. 1985 Computer simulation of granular shear flows. *J. Fluid Mech.* **151**, 167–188.
- CAMPBELL, C. S., CLEARY, P. & HOPKINS, M. A. 1995 Large landslide simulations: global deformation, velocities and basal friction. *J. Geophys. Res.* **100**, 8267–8283.
- CAMPBELL, C. S. & GONG, A. 1986 The stress tensor in a two-dimensional granular shear flow. *J. Fluid Mech.* **164**, 107–125.
- CAMPBELL, C. S. & ZHANG, Y. 1992 Interfaces between fluid-like and solid-like behaviour in granular flows. In *Advances in Micromechanics of Granular Materials – Proc. the Second US/Japan Seminar on the Micromechanics of Granular Materials, Potsdam New York, 5–9 August 1991* (ed. H. H. Shen, M. Satake, M. Mehrabadi, C. S. Chang & C. S. Campbell), pp. 261–70. Elsevier.
- CASAGRANDE, A. 1938 Compaction tests and critical density investigations in cohesionless materials for Franklin Falls dam. *US Engineer Corps, Boston District* **31**, 74–87.
- COULOMB, C. A. 1773 Essai sur un application de règles de maximis et minimis à quelques problèmes de staique relatifs à l'architecture. *Mémoires de Mathématique et de Physique de l'Académie Royale des Sciences*, Paris **7**, 343–82.
- CUNDALL, P. A. & STRACK, O. D. L. 1979 A discrete numerical model for granular assemblies. *Geotechnique* **29**, 47–65.
- DRESCHER, A. & DE JOSSELIN DE JONG, G. 1972 Photoelastic verification of a mechanical model for the flow of a granular material. *J. Mech. Phys. Solids* **20**, 337–351.
- HANES, D. M. & INMAN, D. L. 1985 Observations of rapidly flowing granular fluid flow. *J. Fluid Mech.* **150**, 357–380.
- HERRMANN, H. J. & LUDING, S. 1998 Modeling granular media on the computer. *Cont. Mech. Therm.* **10**, 189–231.
- HOOVER, W. G. 1985 Canonical dynamics: equilibrium phasespace distributions. *Phys. Rev. A* **31**, 1695–6.
- HOPKINS, M. A. & LOUGE, M. Y. 1991 Inelastic microstructure in rapid granular flows of smooth disks. *Phys. Fluids A* **3**, 47–57.
- HOSTLER, S. R. & BRENNEN, C. E. 2003 Granular state effects on wave propagation. *Proc. Mat. Res. Soc. Symp.* **757**, 73–78.
- HOWELL, D. W., BEHRINGER, R. P. & VEJE, C. T. 1999a Fluctuations in granular media. *Chaos* **9**, 559–572.
- HOWELL, D. W., BEHRINGER, R. P. & VEJE, C. T. 1999b Stress fluctuations in a 2D granular Couette experiment: a continuous transition. *Phys. Rev. Lett.* **26**, 5241–5244.
- JACKSON, R. 1983 Some mathematical and physical aspects of continuum models for the motion of granular materials. In *Theory of Dispersed Multiphase Flow* (ed. R. E. Meyer), pp. 291–337, Academic.
- LEES, A. W. & EDWARDS, S. F. 1972 The computer study of transport processes under extreme conditions. *J. Phys. C: Solid State Phys.* **5**, 1921–1929.

- LUN, C. K. K., SAVAGE, S. B., JEFFREY, D. J. & CHEPURNIY, N. 1984 Kinetic theories for granular flow: inelastic particles in Couette flow and slightly inelastic particles in a general flowfield. *J. Fluid Mech.* **140**, 223.
- MILLER, B., O'HERN, C. & BEHRINGER, R. P. 1996 Stress fluctuations for continuously sheared granular materials. *Phys. Rev. Lett.* **77**, 3110–3113.
- MUETH, D. M., JAEGER, H. M. & NAGEL, S. R. 1998 Force distribution in a granular medium. *Phys. Rev. E* **57**, 3164–3169.
- POTAPOV, A. V. & CAMPBELL, C. S. 1996 Computer simulation of hopper flows. *Phys. Fluids A* **8**, 2884–2894.
- RICHART, F. E. JR. 1978 Field and laboratory measurements of dynamic soil properties, in *Dynamic Response and Wave propagation in Soils* (ed. B. Prange). A. A. Balkema, Rotterdam.
- RICHART, F. E., WOODS, R. D. & HALL, J. P. 1970 *Vibration of Soils and Foundations*. Prentice-Hall.
- ROSCOE, K. H., SCHOFIELD, A. N. & WROTH, C. P. 1958 On the yielding of soils. *Geotechnique* **8**, 22–53.
- SAVAGE, S. B. & SAYED, M. 1984 Stresses developed by dry cohesionless granular materials in an annular shear cell. *J. Fluid Mech.* **142**, 391–430.
- SCHOFIELD, A. & WROTH, P. 1968 *Critical State Soil Mechanics*. McGraw-Hill, 310pp.
- WANG, D. G. & CAMPBELL, C. S. 1992 Reynolds' analogy for a shearing granular material. *J. Fluid Mech.* **244**, 527–546.
- ZHANG, Y. & CAMPBELL, C. S. 1992 The interface between fluid-like and solid-like behavior in two-dimensional granular flows. *J. Fluid Mech.* **237**, 541–568.